Materials Advances

ROYAL SOCIETY OF CHEMISTRY

PAPER

View Article Online
View Journal | View Issue

Cite this: *Mater. Adv.*, 2024, 5, 1332

Malic acid-coated iridium nanoparticle-induced cascade enzymatic reactions for norepinephrine detection†

Xuan Chen, Lin Zhou, Zhanghong Guo and Qijun Song *

Received 9th September 2023,
Accepted 17th December 2023

DOI: 10.1039/d3ma00687e

rsc.li/materials-advances

In this work, malic acid (MA) stabilized iridium nanoparticles (MA-IrNPs) were prepared by one-pot synthesis using MA and $IrCl_3$ as the precursors and $NaBH_4$ as the reducing agent. The as prepared MA-IrNPs have exhibited multi-enzyme activities, especially an excellent laccase-like activity and improved environment adaptability. For the substrate 2,4-dichlorophenol (2,4-DP), a low K_m value of 0.117 mM and a high V_{max} value of 0.002 mM s^{-1} were obtained. Under the catalysis of MA-IrNPs, the colourless norepinephrine (NE) can be selectively oxidized by dissolved oxygen to form an orange-brown product and the reaction can be substantially accelerated in the presence of H_2O_2 due to the synchronic effect of catalase-like and laccase-like activity of MA-IrNPs. Based on this chromogenic reaction, a sensitive colourimetric method was developed for the determination of NE in urine samples. A limit of detection as low as 0.05 μM and a wide linear range of 0.1–120 μM were achieved, showing a promising application potential of MA-IrNPs in disease diagnosis.

1 Introduction

As powerful biocatalysts, natural enzymes facilitate most biological reactions that occur in living systems.[1] Currently, they have also been explored for wide applications in the food industry, biomedicine, environmental protection and many other fields. Although substantial progress has been achieved, natural enzymes have also exhibited a number of inherent disadvantages in practical applications, such as their susceptibility to environmental conditions (pH, temperature and salt content), high cost of production and purification, and difficulty in recycling.[2]

To overcome these drawbacks of natural enzymes, nanomaterial-based artificial enzymes, also known as nanozymes, have been studied extensively in recent years.[3] Nanozymes are nanomaterials with intrinsic enzyme-like activity, which have the advantages of high catalytic efficiency,[4] stable performance and tuneable activities.[5,6] Since the first report of Fe_3O_4 nanoparticles with an enzyme mimetic activity by Yan *et al.* in 2007,[7] substantial progress has been achieved in the research on nanozymes. For example, the incorporation of the well dispersed superparamagnetic iron oxide (IO) nanoparticles (NPs) on mesoporous carbon (IO-MC) shows improved peroxidase mimetic activity, which was successfully applied to glucose detection.[8] Yamauchi *et al.* further revealed that the mesoporous γ-Fe_2O_3 exhibits higher peroxidase mimetic activity compared to α-Fe_2O_3.[9]

Among various metallic elements, iridium is known to have superb catalytic activity and excellent stability; hence, iridium-based nanozymes have attracted increasing research interest in recent years.[10] In our previous works, a series of iridium nanozymes were prepared, including tannic acid-coated iridium nanoparticles (TA-IrNPs), citric acid-coated iridium nanoparticles (Cit-IrNPs) and tartaric acid-coated iridium nanoparticles (Tar-IrNPs).[11,12] Based on the laccase activity of Tar-IrNPs, a colourimetric method was developed for the detection and degradation of *o*-phenylenediamine (OPD) and *p*-phenylenediamine (PPD).[13]

It is interesting to note that the IrNPs stabilized with different molecules often exhibit varied enzymatic activities. In our previous study,[14] catalytic performances were comprehensively studied both by experimental characterization and theoretical calculations. It was found that the catalytic properties of the IrNPs are derived from the lattice planes, which are affected by the caption agents during the formation of IrNPs. All the IrNPs could catalyze the degradation of H_2O_2 due to the presence of the Ir (111) plane, while only the IrNPs with the Ir (220) plane exhibit oxidase-like activity. In general, small molecule-stabilized IrNPs, such as Cit-IrNPs and Tar-IrNPs, tend to have multiple enzymatic activities. Furthermore, in

Key Laboratory of Synthetic and Biological Colloids, Ministry of Education, School of Chemical and Material Engineering, Jiangnan University, 1800 Lihu Road, Wuxi, Jiangsu Province 214122, P. R. China. E-mail: qsong@jiangnan.edu.cn; Fax: +0086-510-85917763; Tel: +0086-510-85700165

† Electronic supplementary information (ESI) available. See DOI: https://doi.org/10.1039/d3ma00687e

contrast to carboxyl groups, the presence of hydroxyl groups in the coating agent is beneficial for the nucleophilicity of the nanozymes.[15,16] Malic acid (2-hydroxybutanedioic acid, MA) has two carboxyl groups and small molecular weight, and hence it is selected as the stabilizer in the present work. As expected, the resultant MA-IrNPs exhibited excellent oxidase, peroxidase, catalase and laccase activities. In particular, MA-IrNPs possessed higher affinity for laccase substrates when compared with that of Tar-IrNPs. The catalytic activity and stability of MA-IrNPs were also substantially better than that of natural laccase. This specific feature is manifested by their effective catalysis on the chromogenic reaction between catecholamine compounds and dissolved oxygen. Due to MA-IrNPs also possessing excellent catalase-like activity, the addition of H_2O_2 can substantially accelerate the chromogenic reaction due to the increased supply of oxygen in the reaction system. Based on the cascade enzymatic reactions, a sensitive colourimetric method was developed for the determination of NE. NE is a catecholamine neurotransmitter secreted by noradrenergic neurons in the sympathetic and central nervous systems.[17] Abnormally elevated levels of NE can be used as a clinical diagnostic for certain diseases, such as pheochromocytoma and paraganglioma.[18] Conventional analytical methods are available for NE analysis;[19] however, they often require expensive equipment, and complicated and prolonged sample pretreatments. Therefore, it is of great significance to develop a simple and low-cost method for the determination of NE.

2 Experimental section

2.1 Materials

Iridium(III) chloride trihydrate ($IrCl_3{\cdot}xH_2O$), sodium hydroxide, 3,3,5,5-tetramethylbenzidine (TMB), sodium borohydride ($NaBH_4$), sodium acetate anhydrous and acetic acid were obtained from Aladdin Chemicals Co. Ltd (Shanghai, China). Sodium acetate, acetic acid, *p*-benzoquinone, L-tryptophan, MA, NE, isopropyl alcohol, hydrogen peroxide (H_2O_2, 30%), 4-aminoantipyrine (4-AP) and 2,4-DP were purchased from Sinopharm Chemical Reagent Co. Ltd (China). All reagents were of analytical grade and were used without further purification. Milli-Q ultra-pure water (18.2 MΩ cm) was used throughout the experiments.

2.2 Characterizations

The absorption spectra and kinetic assay were conducted on a UV-vis spectrophotometer (UV-2700, Japan Shimadzu). The surface morphology of the samples was observed on a transmission electron microscope (TEM, JEOL, JEM-2100plus). The oxidation state of iridium and the interaction with MA were analyzed by X-ray photoelectron spectroscopy (XPS) using a PHI Quantum 2000 Scanning ESCA Microprobe. Fourier transform infrared spectra (FT-IR) were recorded on a Fourier infrared spectrometer (Nicolet iS50 FT-IR, Thermo Fisher Scientific, USA). The XRD analysis was performed on an XRD spectrometer (D8, Bruker AXS, Germany) with Cu-Kα radiation and 2θ was scanned from 5° to 90° at 5° min^{-1}. The pH and dissolved oxygen were measured with a DZS708 L Multiparameter analyzer (Shanghai INESA Scientific Instrument Co. Ltd, China).

2.3 Preparation of the MA-IrNPs

The MA-IrNPs were synthesized by a simple one-pot method using iridium(III) chloride ($IrCl_3{\cdot}xH_2O$) and MA as the precursors. Briefly, an aliquot of 10 mL of 2 mM $IrCl_3$ solution was mixed with 20 mL of 16 mM MA solution. The mixture was adjusted to pH 6–7 with NaOH and heated to reflux for 30 min under vigorous stirring. After that, freshly prepared $NaBH_4$ solution was added and the heater was turned off. Constant stirring was continued until the reaction mixture cooled to room temperature, during which the colour of the reaction mixture gradually changed from light yellow to deep blue, indicating the formation of nanoparticles. The formed nanoparticles were purified by the addition of ethanol to the reaction solution (2 : 1 volume ratio) and centrifuged at 10 000 rcf for 8 min. The final product was obtained by repeatedly washing the precipitate and dried at 45 °C in a vacuum oven. Then, 3.0 mg MA-IrNPs were added to 3.0 mL of water and ultrasonically dispersed for 10 min for further use.

2.4 Multienzyme activity of MA-IrNPs

2.4.1 Assessment of the oxidase-like activity of MA-IrNPs. The oxidase-like properties of MA-IrNPs were evaluated by using TMB as a chromogenic substrate. In a typical procedure, the experiment was conducted in acetate buffer solution (0.1 M pH = 4) containing 8 μg mL^{-1} MA-IrNPs and various concentrations of TMB. The rate of TMB oxidation was monitored by recording the absorbance at 652 nm.

2.4.2 Assessment of the catalase-like and peroxidase-like activity of MA-IrNPs. To investigate the catalase-like activity of MA-IrNPs, an aliquot of 30 μL of 1.2 mg mL^{-1} MA-IrNPs solution was added to 20 mL of 20 mM H_2O_2 solution, and the change of dissolved oxygen concentration was monitored with a multi-parameter analyzer equipped with an oxygen electrode.

In the peroxidase-like activity assay, 5 μL of 10 μg mL^{-1} MA-IrNPs, 50 μL of 0.1 M TMB, and 10 μL of 0.1 M H_2O_2 were sequentially added in 935 μL of 0.1 M acetate buffer solution (pH = 3.8). The absorbance of the reaction system was recorded at 652 nm using a UV-vis spectrophotometer.

2.4.3 Assessment of the laccase-like activity of MA-IrNPs. The laccase-like activity of the MA-Ir NPs was evaluated by the classical chromogenic reaction of 2,4-DP and 4-AP.[20] Briefly, 40 μL of 1 mg mL^{-1} MA-IrNPs solution was mixed with 2,4-DP (1 mg mL^{-1} 100 μL), 4-AP (1 mg mL^{-1} 100 μL) and 760 μL acetate buffer solution (0.1 M pH = 7). After 10 min of reaction at room temperature, the absorbances were recorded at 510 nm. To determine the reaction rates, various concentrations of 2,4-DP (10–60 μg mL^{-1}), 4-AP (1 mg mL^{-1} 100 μL), and MA-Ir NPs (1 mg mL^{-1} 40 μL) were used for the reactions. The kinetic parameters were calculated based on the Michaelis–Menten equation:[21]

$$\frac{1}{V} = \frac{K_m}{V_{max}} \times \frac{1}{c} + \frac{1}{V_{max}}$$

where V is the initial reaction rate, K_m is the Michaelis–Menten constant, V_{max} is the initial maximum reaction rate, and c is the substrate concentration.

2.5 The effect of pH and temperature on the laccase-like activity of MA-IrNPs

The catalytic activities of MA-IrNPs and natural laccase were investigated under different pH and temperature conditions. To study the influence of reaction pH, 100 μL of 4-AP solution (1 mg mL^{-1}) and 100 μL of 2,4-DP solution (1 mg mL^{-1}) were mixed with 760 mL of acetate buffer solutions with different pH (2–11). Then, 40 μL of MA-IrNPs solution (1 mg mL^{-1}) or 40 μL of natural laccase solution (250 mg mL^{-1}) was added to the mixture. After 10 min of reaction, the absorbance at 510 nm was recorded. Similarly, the influence of reaction temperature on MA-IrNPs and natural laccase was studied in acetate buffer (0.1 M pH = 7) with the reaction temperature varied from 20 °C to 90 °C.

2.6 Salt effect and storage stability

To investigate the effect of ionic strength on the enzymatic activity, different kinds of salts ($NaNO_3$, NaCl and KCl) were added to the reaction mixture of 2,4-DP, 4-AP and MA-IrNPs or natural Laccase, and the absorbance was recorded after 10 min reaction. Likewise, to study storage stability, MA-IrNPs and natural laccase solutions were stored at room temperature, and their catalytic activities were evaluated every ten days.

2.7 Colourimetric determination of NE in urine based on the cascade catalase-like and laccase-like enzymatic reactions

For NE analysis, an aliquot of 30 μL of MA-IrNPs (1 mg mL^{-1}), 10 μL of 0.1 M H_2O_2 and 10 μL of different concentrations of NE were sequentially added in 950 μL of 0.01 M acetate buffer solution (pH = 7). After thorough mixing, the absorbance at 485 nm was recorded and the dissolved oxygen concentration was monitored with a multi-parameter analyzer equipped with an oxygen electrode. For real sample analysis, urine samples from healthy volunteers were collected. The standard addition method was used to evaluate the recovery of our method. The spiked samples were diluted 5 times with buffer solution, and then the concentrations of NE were measured by the colourimetric method.

3 Results and discussion

3.1 Preparation and characterization of MA-IrNPs

Our previous studies have revealed that carboxyl and hydroxyl groups on the coating agents have a great influence on the formation of IrNPs due to their different complexing capability to Ir^{3+}. It was found that the IrNPs synthesized with small molecule stabilizers with multiple carboxyl groups exhibited greater catalytic activity, presumably because IrNPs stabilized with small molecules should have more exposed active sites.[12] Compared with the Tar used in our previous work, MA also has two carboxyl groups but with smaller molecular weight, and thus MA was selected as the coating agent in the present work. As expected, the MA-IrNPs were facilely prepared with one-pot reaction in aqueous solution, and the resultant nanoparticles can be precipitated from the solution by the addition of ethanol. After centrifugation washing and drying, a deep blue coloured powder was obtained. As shown in the TEM images in Fig. 1A, the average particle size of the synthesized nanoparticles was 1.1 nm. The HRTEM in Fig. 1B further reveals the morphology of the MA-IrNPs, and the lattice stripes on the surface can be clearly observed. Fig. 1C shows the XRD spectrum, where the main diffraction peaks of 2θ are 40.71°, 47.27°, 69.15° and 83.45°, corresponding to the four crystalline planes Ir{111}, Ir{200}, Ir{220}, and Ir{311}, respectively.[22,23]

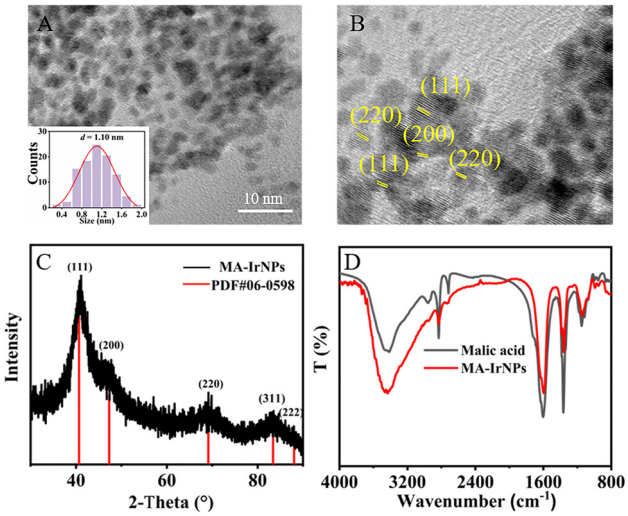

Fig. 1 Structural characterization of MA-IrNPs. (A) TEM image (inset: particle size distribution) (B) HRTEM image, (C) XRD pattern of MA-IrNPs and (D) FT-IR spectra of MA and MA-IrNPs.

The XPS spectrum was used to characterize the element valence and binding on the surface of the MA-IrNPs. Fig. 2A shows the three peaks of Ir 4f, O 1s, and C 1s. The fine pattern of Ir 4f can be found in Fig. 2B, and the peaks at 60.61 and 63.4 eV correspond to the binding energy of $4f_{7/2}$ and $4f_{5/2}$ of Ir (0) respectively[24] and the peaks at 61.7 and 65.8 eV correspond to $4f_{7/2}$ and $4f_{5/2}$ of $Ir^{\delta+}$–O.[25] The O 1s spectrum of MA-IrNPs has two peaks (Fig. 2C), which can be attributed to –C═O (531.2 eV) and $Ir^{\delta+}$–O (532.8 eV), respectively. Fig. 2D depicts the C 1s spectrum of MA-IrNPs, where the three peaks at 284.45 eV, 287.98 eV and 532.8 eV belong to C–C, $C–OH_{alch}$[26] and coordinated carboxylates (COO–Ir),[27] respectively. Based on these XPS data, it can be seen that both Ir (0) and $Ir^{\delta+}$ are presented on the MA-IrNP surface. The zeta potential of the MA-IrNPs was measured to be −50.8 mV (Fig. S1, ESI†), which indicates that the surface of the MA-IrNPs is negatively charged. The absolute value is greater than 20 mV, suggesting that MA-IrNPs are stabilized in aqueous solution by electrostatic repulsion. These characterizations suggest that the carboxyl groups on the surface of MA bind to the nanoparticles *via* COO–Ir. This consumption can be further confirmed by the FT-IR of MA-IrNPs (Fig. 1D), and the telescopic vibrational peaks ν_{asy}(COO) and

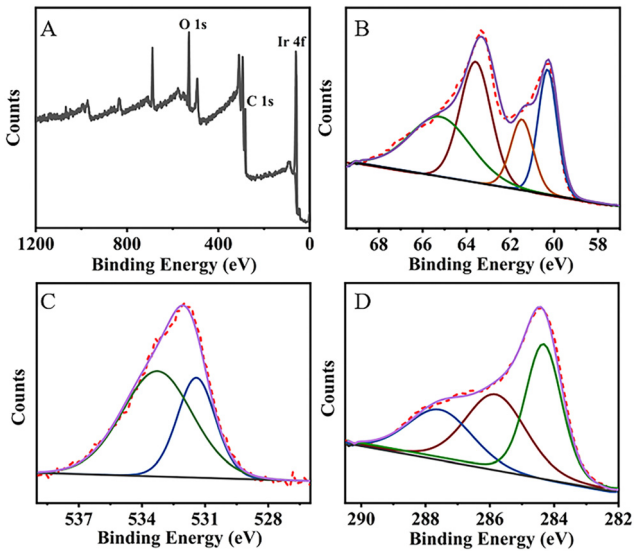

Fig. 2 The XPS analysis of MA-IrNPs. (A) Full scan spectrum, (B) Ir 4f spectrum, (C) O 1s spectrum and (D) C 1s spectrum.

ν_{sym}(COO) of the carboxylate group of MA can be observed at 1595 cm^{-1} and 1348 cm^{-1}.[28–30] The difference between the peak positions ($\Delta\nu$) corresponds to the coordination mode between the metal ions and the carboxylate.[31] The value of $\Delta\nu$ is 235 cm^{-1}, which implied that the carboxylate group of MA forms a single-type coordination on the surface of the IrNPs.

3.2 The oxidase-like, peroxidase-like, and catalase-like activity of MA-IrNPs

TMB was chosen as a substrate to evaluate the oxidase-like activity of MA-IrNPs. In the presence of MA-IrNPs, TMB was oxidized by dissolved oxygen to blue oxTMB with a strong absorption peak at 652 nm. In contrast, TMB cannot be oxidized by dissolved oxygen to form the blue coloured oxTMB in the absence of MA-IrNPs, indicating that MA-Ir NPs have oxidase-like activity and can directly catalyze the oxidation of TMB by dissolved oxygen (Fig. 3A). The steady-state kinetics demonstrated that the catalytic oxidation of TMB by MA-IrNPs follows the Michaelis–Menten behaviour. As shown in Fig. S2 (ESI†), the data were fitted to the Lineweaver–Burk equation, and the K_m and V_{max} were calculated to be 0.215 mM and 0.001 mM s^{-1}, respectively. Fig. 3B shows the peroxidase-like activity of the MA-IrNPs, and the mixture exhibits a clear colour change in the presence of H_2O_2. It is worth noting that the dosage of MA-IrNPs used for the peroxidase activity study was substantially lower than that used in the oxidase activity test, and only a ng mL^{-1} level of MA-IrNPs was enough to exhibit strong peroxidase performance. Furthermore, MA-IrNPs also exhibit intrinsic catalase-like activity, which can accelerate the decomposition of H_2O_2 and produce O_2 simultaneously. As shown in the inset of Fig. 3C, a large number of bubbles was generated in the solution and the dissolved oxygen content was increased steadily upon the addition of MA-IrNPs to H_2O_2 aqueous solution.

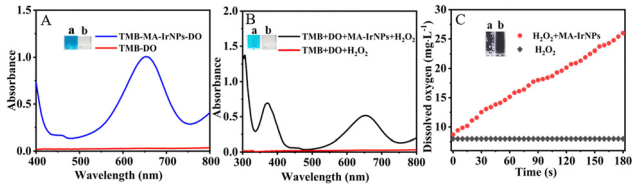

Fig. 3 (A) The absorption spectra of the TMB-DO-MA-IrNPs and TMB-DO system (inset: digital photos of (a) TMB-DO-MA-IrNPs and (b) TMB-DO). (B) The absorption spectra of MA-IrNPs-TMB-DO-H_2O_2 and TMB-DO-H_2O_2 (inset: digital photos of (a) MA-IrNPs-TMB-DO-H_2O_2 and (b) TMB-DO-H_2O_2). (C) The change of DO content over time with and without MA-IrNPs (inset: digital photos of (a) MA-IrNPs-H_2O_2 and (b) H_2O_2).

3.3 The laccase-like activity of the MA-IrNPs

The laccase-like activity of MA-IrNPs was evaluated using 2,4-DP as a substrate and 4-AP as a chromogenic reagent.[32] 2,4-DP is a substance with a polyphenolic structure that can be oxidized by dissolved oxygen under the catalysis of laccase and laccase-like enzymes. The oxidation products of 4-AP and 2,4-DP undergo a condensation reaction to give a red coloured product with a strong absorption at 510 nm[33] (Fig. 4A). As shown in Fig. 4A, no absorption peak appeared on the UV-vis spectrum in the absence of the catalyst, and the chromogenic reaction also did not proceed by mixing MA-IrNPs with 2,4-DP or 4-AP, respectively. In the presence of 2,4-DP, 4-AP and MA-IrNPs, a burgundy coloured product was formed with its maximum absorption at 510 nm, suggesting that the MA-IrNPs possess a laccase-like activity.

By replacing MA-IrNPs with natural laccase, the enzyme activity of natural laccase was also evaluated by the same method. In brief, 250 mg of natural laccase was added to

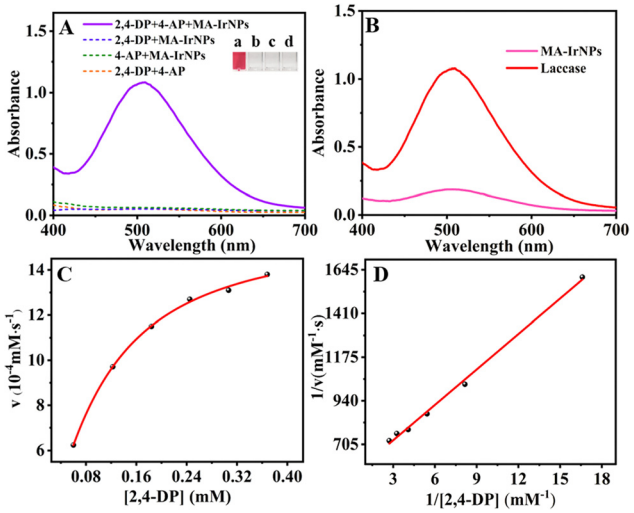

Fig. 4 (A) The absorption spectra of the MA-IrNPs + 2,4-DP + 4-AP, and without the MA-IrNPs, 2,4-DP or 4-AP, respectively (inset: digital photos of (a) MA-IrNPs + 2,4-DP + 4-AP, (b) MA-IrNPs + 4-AP, (c) MA-IrNPs + 2,4-DP and (d) 2,4-DP + 4-AP). (B) Catalytic activities of MA-IrNPs and natural laccase. (C) Steady state kinetic assay of laccase-like activity of MA-IrNPs. (D) Double-reciprocal plots of the laccase-like activity of MA-IrNPs.

1 mL of water and ultrasonically dispersed for 10 min. Then, 40 μL of 250 mg mL^{-1} natural laccase solution was added to the reaction system and the absorbances were recorded after 10 min. Fig. 4B shows that a similar chromogenic reaction was observed but with a relatively low absorbance. And the absorbance at 510 nm was only 17% of that measured from MA-IrNPs even with the amount of natural laccase being 250 times the amount of MA-IrNPs. In addition, Fig. S4 (ESI†) shows that the absorbance at 510 nm increases with time, but the increase rate obtained from MA-IrNPs is significantly greater than that obtained from natural laccase. These results demonstrated that MA-IrNPs have a much higher catalytic activity than that of natural laccase. The catalytic characteristics of MA-IrNPs were further investigated and the results are presented in Fig. 4C and D. According to the experimental data, the calculated K_m for the substrate 2,4-DP is 0.117 mM, which is remarkably lower than that obtained from natural laccase (Table S1, ESI†). MA-IrNPs also exhibit a higher V_{max} (0.002 mM s^{-1}) than that of natural laccase (Table S1, ESI†).[34] Hence, compared with natural laccase, the MA-IrNPs prepared in this work exhibits a higher catalytic activity and better affinity for substrates. The MA-IrNPs also show an improved enzymatic activity than that of Tar-IrNPs, as less MA-IrNPs (40 μg mL^{-1}) were required in the same chromogenic reaction. Furthermore, a smaller value of K_m means that the catalyst has a greater affinity for the substrate. By comparing the kinetic parameters between MA-IrNPs and Tar-IrNPs, the calculated K_m value and V_m are 0.117 mM and 2.0 × 10^{-3} mM s^{-1}, respectively for MA-IrNPs, and 0.204 mM and 5.4 × 10^{-3} mM s^{-1} for Tar-IrNPs (Table S1, ESI†). All these results demonstrate that MA-IrNPs have better laccase-like activity than Tar-IrNPs.

3.4 Catalytic stability of MA-IrNPs

The catalytic stability is an important criterion for the practical application of a catalyst. Hence the influences of pH, temperature, ionic strength and storage time on the catalytic activity of MA-IrNPs were evaluated with the chromogenic reaction of 2,4-DP and 4-AP. Fig. 5A shows that the highest catalytic activity was observed at 60 °C and further increase or decrease in temperature could lead to a decline in the enzymatic activity. However, a relatively high enzymatic activity can be obtained with MA-IrNPs across a wide temperature range of 30–80 °C, whereas the performance of the laccase decreases sharply above and below 60 °C. Fig. 5B exhibits that for both MA-IrNPs and laccase, the optimum pH was in the neutral condition (pH = 7). Again, compared to natural laccase, MA-IrNPs have shown better performance under more acidic or alkaline conditions. As shown in Fig. 5B, MA-IrNPs maintained more than 60% catalytic activity at pH = 11, but the natural laccase had basically lost its catalytic activity at pH = 9. These results demonstrate that MA-IrNPs have higher pH and temperature stability compared to natural laccase.

Fig. 5C shows that the catalytic activity of natural laccase decreased sharply even when stored at room temperature and only 10% of their initial activity can be retained after 20 days. In contrast, MA-IrNPs present high storage stability, and above

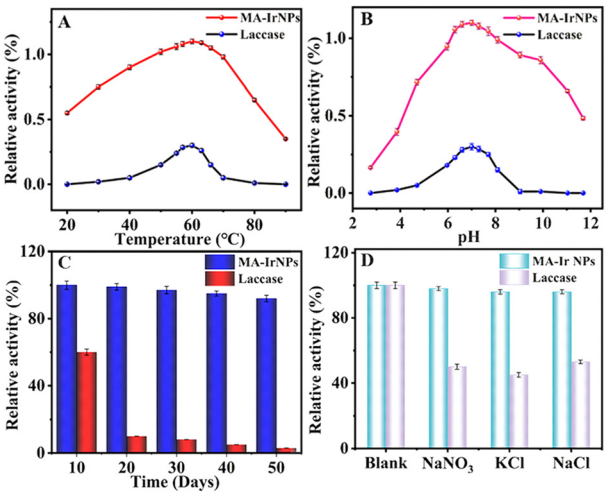

Fig. 5 (A) Comparison of MA-IrNPs and natural laccase activities at different temperatures. (B) Comparison of MA-IrNPs and natural laccase activities in different pH acetate buffer solution. (C) Comparison of the relative catalytic activities of MA-IrNPs and natural laccase at different storage times. (D) Comparison of the relative catalytic activities of MA-IrNPs and natural laccase in the presence of different salt ion concentrations.

90% of their catalytic activity was maintained even after 50 days of storage. Fig. 5D presents the salt effect on the catalytic activity of natural laccase and MA-IrNPs. It can be seen that the activity of natural laccase decreased sharply in the presence of 150 mM NaCl, KCl and $NaNO_3$ presumably due to the inhibition effect of Cl^- and NO_3^-.[34] Compared to natural laccase, the performance of MA-IrNPs was largely unaffected in the presence of 150 mM NaCl, KCl and $NaNO_3$, indicating its good catalytic stability under high salinity.

3.5 Catalytic mechanism of MA-Ir NPs

Natural laccase is a copper blue oxidase that catalyzes the substrate oxidation by oxygen *via* direct electron transfer processes.[35] Solomon *et al.* studied the catalytic mechanism of natural laccase, and thought copper clusters were the main active sites.[36] The adsorption of the substrate on the catalyst could promote the four electron reduction of O_2 to H_2O.[37] In the present work, the effect of oxygen was preliminarily investigated in different reaction atmospheres. Fig. S3A (ESI†) shows that the MA-IrNPs catalyzed reaction can be dramatically inhibited by bubbling N_2 gas into the system, indicating that O_2 was essential in the oxidation process. The free radical quenching experiments were carried out to explore the possible involvement of reactive oxygen species. *p*-Benzoquinone (5 mM), *tert*-butanol (5 mM) and L-histidine (5 mM) were respectively applied as the scavengers of $^{\bullet}O_2^-$,[38] $^{\bullet}OH$[39] and $^1O_2$.[40] Fig. S3B (ESI†) shows that the addition of these scavengers had little effect on the chromogenic reaction, which rules out the involvement of these reactive oxygen species in the MA-IrNP catalyzed oxidation of the substrates. Therefore, an electron transfer process is more likely to be the key route for the oxidation of the phenolic substrates, *i.e.*, the reaction

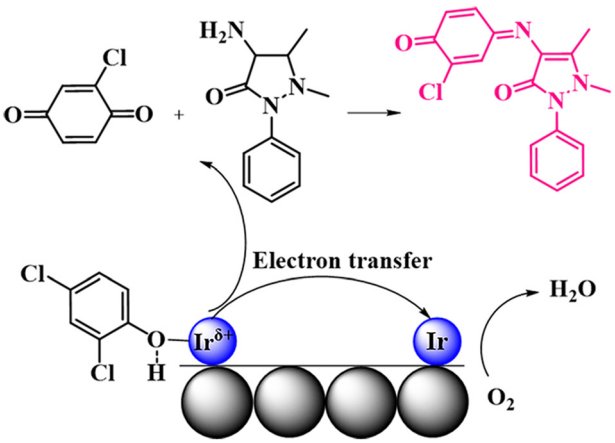

Fig. 6 The mechanism for the oxidation of 2,4-DP under catalysis of MA-IrNPs.

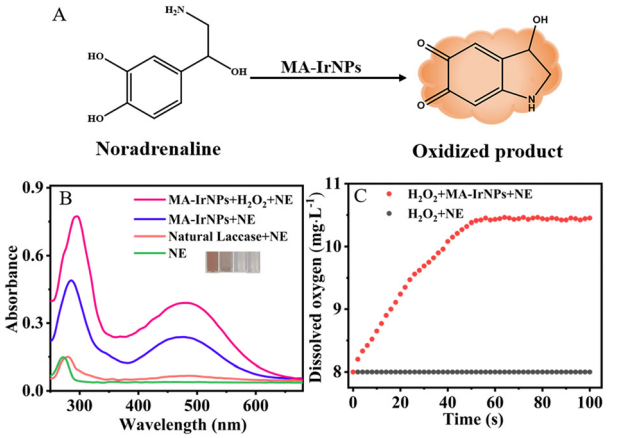

Fig. 7 (A) The colourimetric reaction of NE catalyzed by MA-IrNPs. (B) Oxidation of NE under different catalyst conditions. (C) The change of DO content over time with and without MA-IrNPs in H_2O_2 and NE.

mechanism is consistent with that of natural laccase. The electron transfer process for the oxidation of 2,4-DP under catalysis of MA-IrNPs was tentatively proposed in Fig. 6. MA-IrNPs have both Ir (0) and $Ir^{\delta+}$ on their surfaces according to the XPS data. The substrate 2,4-DP bound to $Ir^{\delta+}$ on the surface of MA-IrNPs facilitated the subsequent oxidation of 2,4-DP to form quinone compounds. Then these quinone compounds reacted with 4-AP to form red-coloured products. At the same time, oxygen is reduced to H_2O through obtaining electrons from the Ir (0) on the surface of the IrNPs, which is re-oxidized to form $Ir^{\delta+}$, and thus the catalytic reaction can proceed *via* the electron cycling between $Ir^{\delta+}$ and Ir (0), and only dissolved oxygen is consumed in this process.

3.6 Colourimetric detection of NE in urine based on the cascade reaction of catalase-like and laccase-like activity

NE is a catecholamine hormone that plays an important role in the physiological processes of stress, anxiety, sleep and memory. Abnormal increase in NE levels can be a clinical indicator for a range of diseases such as pheochromocytoma and paraganglioma.[41] Therefore, rapid and accurate determination of NE is of great importance in medical diagnosis. NE is a polyphenol that can be catalytically oxidized to produce an orange-brown product with its absorption peaked at 485 nm (Fig. 7A and B). It can also be observed from Fig. 7B that the catalytic efficiency of MA-IrNPs is substantially greater than that of natural laccase. As MA-IrNPs also possess catalase-like activities, H_2O_2 was added to the system to induce the production of more oxygen in the oxidation reaction. Fig. 7C shows that the concentration of dissolved oxygen was increased and maintained at a high level. Consequently, the absorption peak of the oxidation products is markedly increased in the presence of H_2O_2 (Fig. S5, ESI†). Based on these cascade reactions, a colourimetric method for the determination of NE was established. As shown in Fig. 8A, the absorbance at 485 nm increased with increasing concentration of NE, and the colour changes can be distinguished by the naked eye. A good linear relationship between the absorbance and the concentration of

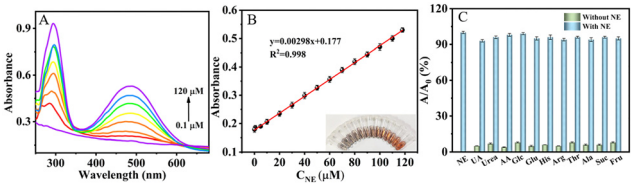

Fig. 8 (A) Absorption spectra of different concentrations (0.1–120 μM) of NE. (B) Linear plot for the determination of NE (inset: the actual colour changes). (C) The anti-interference study for colourimetric determination of NE.

NE was established in the range of 0.1–120 μM (Fig. 8B), and a limit of detection (LOD) as low as 50 nM was obtained based on the 3σ criterion. The detection limits and linear ranges obtained from MA-IrNPs are substantially better than that of other reported works.[42]

To further investigate the selectivity of the MA-IrNP colourimetric assay for NE, we investigated the effect of various interferents such as urea, glucose, ascorbic acid, uric acid and amino acids on the determination of NE. As shown in Fig. 8C, the addition of these interferents had no significant effect on the colorimetric determination of NE, which shows that the method has good selectivity for the determination of NE.

To test the practical applicability, we measured the concentration of NE in real human urine samples by the standard sample addition method. As shown in Table 1, the recovery rates of NE were within the range of 98–103%, and the relative standard deviation (RSD) was less than 3.1% for all the samples. These results show that the MA-IrNP-catalyzed colourimetric method is highly reliable for the determination of NE in real samples.

4 Conclusions

In summary, malic acid-stabilized iridium nanoparticles (MA-IrNPs) were prepared by the one-pot synthetic method and the

Table 1 Determination of NE in human urine samples by the standard addition method

	Added (μM)	Found (μM)	Recovery (%)	RSD (%, n = 3)
NE	0.9	0.92	102.2	2.2
	5	4.98	99.6	1.9
	10	9.81	98.1	3.1
	20	20.06	100.3	2.6

obtained MA-IrNPs have shown improved enzymatic activity compared with other previously reported nanozymes and natural laccase. The results confirm that the stabilizer with small molecular weight and multiple carboxyl groups is beneficial for the preparation of IrNPs with good enzymatic performance. Mechanistic study reveals that the laccase-like activity of MA-IrNPs originates from catalyst accelerated electron transfer between the substrate and dissolved oxygen. Oxygen generation from the decomposition of H_2O_2 by the catalase property of MA-IrNPs can further promote the oxidation of NE. Based on the catalysis of MA-IrNPs, a colourimetric method for the determination of NE was developed, which not only has high sensitivity and a wide calibration range, but also showed a good selectivity for the determination of NE, due to the high adsorption affinity of NE on the surface of MA-IrNPs. Hence, the results obtained in this work could provide a practical guide for the selection of the capping agent in nanozyme preparation, and the obtained IrNPs have also shown promising application potential in the sensing of important biomolecules with nanozymes.

Author contributions

Miss Xuan Chen carried out the experiments and wrote the first draft of the manuscript. Mr Lin Zhou and Miss Zhanghong Guo were involved in planning the work and performing the data analysis. The corresponding author Prof. Qijun Song was in charge of the overall work and finalized the manuscript.

Conflicts of interest

There are no conflicts to declare.

Acknowledgements

This work is supported by the National First-Class Discipline Program of Food Science and Technology (JUFSTR20180301) and Fundamental Research Funds for the Central Universities (JUSRP22027).

Notes and references

1 R. Zhang, X. Yan and K. Fan, *Acc. Mater. Res.*, 2021, **2**, 534–547.
2 Z. Gao, M. Xu, M. Lu, G. Chen and D. Tang, *Biosens. Bioelectron.*, 2015, **70**, 194–201.
3 H. Wei and E. Wang, *Chem. Soc. Rev.*, 2013, **42**, 6060–6093.
4 J. Wu, X. Wang, Q. Wang, Z. Lou, S. Li, Y. Zhu, L. Qin and H. Wei, *Chem. Soc. Rev.*, 2019, **48**, 1004–1076.
5 K. Korschelt, M. N. Tahir and W. Tremel, *Chemistry*, 2018, **24**, 9703–9713.
6 F. Zheng, W. Ke, L. Shi, H. Liu and Y. Zhao, *Anal. Chem.*, 2019, **91**, 11812–11820.
7 L. Gao, J. Zhuang, L. Nie, J. Zhang, Y. Zhang, N. Gu, T. Wang, J. Feng, D. Yang, S. Perrett and X. Yan, *Nat. Nanotechnol.*, 2007, **2**, 577–583.
8 M. A. Wahab, S. M. A. Hossain, M. K. Masud, H. Park, A. Ashok, M. Mustapić, M. Kim, D. Patel, M. Shahbazi, M. S. A. Hossain, Y. Yamauchi and Y. V. Kaneti, *Sens. Actuators, B*, 2022, **366**, 131980.
9 M. K. Masud, J. Kim, M. M. Billah, K. Wood, M. J. A. Shiddiky, N.-T. Nguyen, R. K. Parsapur, Y. V. Kaneti, A. A. Alshehri, Y. G. Alghamidi, K. A. Alzahrani, M. Adharvanachari, P. Selvam, M. S. A. Hossain and Y. Yamauchi, *J. Mater. Chem. B*, 2019, **7**, 5412–5422.
10 J. Quinson, *Adv. Colloid Interface Sci.*, 2022, **303**, 102643.
11 M. Cui, J. Zhou, Y. Zhao and Q. Song, *Sens. Actuators, B*, 2017, **243**, 203–210.
12 G. Jin, J. Liu, C. Wang, W. Gu, G. Ran, B. Liu and Q. Song, *Appl. Catal., B*, 2020, **267**, 118725.
13 S. Hao, C. Fu, L. Zhou, Z. Guo and Q. Song, *J. Mater. Chem. B*, 2023, **11**, 2770–2777.
14 G. Jin, G. Sun, C. Fu, C. Wang, G. Ran and Q. Song, *Catal. Sci. Technol.*, 2022, **12**, 1017–1024.
15 J. Huo, J. Hao, J. Mu and Y. Wang, *ACS Appl. Bio Mater.*, 2021, **4**, 3443–3452.
16 Z. Liu, S. Gong, Y. Wang, T. Chen, Y. Niu and Y. Xu, *ACS Appl. Bio Mater.*, 2020, **3**, 1459–1468.
17 M. W. Schwartz, S. C. Woods, D. Porte, R. J. Seeley and D. G. Baskin, *Nature*, 2000, **404**, 661–671.
18 S. Casadio, J. W. Lowdon, K. Betlem, J. T. Ueta, C. W. Foster, T. J. Cleij, B. van Grinsven, O. B. Sutcliffe, C. E. Banks and M. Peeters, *Chem. Eng. J.*, 2017, **315**, 459–468.
19 T. Kanamori, T. Funatsu and M. Tsunoda, *Analyst*, 2016, **141**, 2568–2573.
20 J. Guan, M. Wang, R. Ma, Q. Liu, X. Sun, Y. Xiong and X. Chen, *Sens. Actuators, B*, 2023, **375**, 132972.
21 Y. Shen, X. Gao, H. Chen, Y. Wei, H. Yang and Y. Gu, *J. Hazard. Mater.*, 2023, **451**, 131171.
22 L. Feng, Z. Dong, C. Liang, M. Chen, D. Tao, L. Cheng, K. Yang and Z. Liu, *Biomaterials*, 2018, **181**, 81–91.
23 F. Yang, L. Fu, G. Cheng, S. Chen and W. Luo, *J. Mater. Chem. A*, 2017, **5**, 22959–22963.
24 H. Su, D. D. Liu, M. Zhao, W. L. Hu, S. S. Xue, Q. Cao, X. Y. Le, L. N. Ji and Z. W. Mao, *ACS Appl. Mater. Interfaces*, 2015, **7**, 8233–8242.
25 W. Du, J. Wang, L. Zhou, J. Zhou, L. Feng, C. Dou, Q. Zhang, X. Zhang, Q. Zhao, X. Cai, J. Wu, Y. Zheng and Y. Li, *Acta Biomater.*, 2023, **166**, 524–535.
26 C. J. May, H. E. Canavan and D. G. Castner, *Anal. Chem.*, 2004, **76**, 1114–1122.
27 F. Tielens, V. Humblot, C. M. Pradier, M. Calatayud and F. Illas, *Langmuir*, 2009, **25**, 9980–9985.

28 F. Taube, B. Drobot, A. Rossberg, H. Foerstendorf, M. Acker, M. Patzschke, M. Trumm, S. Taut and T. Stumpf, *Inorg. Chem.*, 2019, **58**, 368–381.
29 A. Valverde, G. I. Tovar, N. A. Rio-López, D. Torres, M. Rosales, S. Wuttke, A. Fidalgo-Marijuan, J. M. Porro, M. Jiménez-Ruiz, V. García Sakai, A. García, J. M. Laza, J. L. Vilas-Vilela, L. Lezama, M. I. Arriortua, G. J. Copello and R. Fernández de Luis, *Chem. Mater.*, 2022, **34**, 9666–9684.
30 J. J. Max and C. Chapados, *J. Phys. Chem. A*, 2002, **106**, 6452–6461.
31 C. Ohe, H. Ando, N. Sato, Y. Urai, M. Yamamoto and K. Itoh, *J. Phys. Chem. B*, 1999, **103**, 435–444.
32 A. Koyappayil, H. T. Kim and M. H. Lee, *J. Hazard. Mater.*, 2021, **412**, 125211.
33 Y. Lin, F. Wang, J. Yu, X. Zhang and G. P. Lu, *J. Hazard. Mater.*, 2022, **425**, 127763.
34 J. Wang, R. Huang, W. Qi, R. Su, B. P. Binks and Z. He, *Appl. Catal., B*, 2019, **254**, 452–462.
35 M. Sun, Y. Dang, R. Du, Z. Lu, Y. Wang, X. Wang, C. Song, T. Liu, G. Wang, J. Ye and H. Rao, *Chem. Eng. J.*, 2021, **425**, 130586.
36 S. M. Jones and E. I. Solomon, *Cell. Mol. Life Sci.*, 2015, **72**, 869–883.
37 F. Gao, Z. Xiong, Y. Jia, H. Li and J. Li, *J. Colloid Interface Sci.*, 2022, **628**, 935–942.
38 C. Fu, M. Zhao, X. Chen, G. Sun, C. Wang and Q. Song, *Appl. Catal., B*, 2023, **332**, 122752.
39 G. Yin, C. Fu, F. Zhang, T. Wu, S. Hao, C. Wang and Q. Song, *J. Alloys Compd.*, 2023, **937**, 168382.
40 C. Zhao, W. Gu, C. Wang, S. Sun, H. Zhou, G. Ran and Q. Song, *Anal. Chem.*, 2019, **91**, 12255–12259.
41 T. M. Godoy-Reyes, A. M. Costero, P. Gaviña, R. Martínez-Máñez and F. Sancenón, *ACS Appl. Nano Mater.*, 2019, **2**, 1367–1373.
42 L. Yang, X.-Y. Guo, Q.-H. Zheng, Y. Zhang, L. Yao, Q.-X. Xu, J.-C. Chen, S.-B. He and W. Chen, *Sens. Actuators, B*, 2023, **393**, 134165.